Available online at www.sciencedirect.com
ScienceDirect
Physica D 235 (2007) 29–32
PHYSICA D
www.elsevier.com/locate/physd

Spontaneous buckling of elastic sheets with a prescribed non-Euclidean metric

Efi Efrati, Yael Klein, Hillel Aharoni, Eran Sharon*

The Racah Institute of Physics, The Hebrew University of Jerusalem, Jerusalem 91904, Israel

Available online 24 August 2007

Abstract

We present an experimental study of the three-dimensional (3D) configurations that result from non-uniform lateral growth/shrinking of thin elastic sheets. We build gel sheets that undergo inducible differential shrinking. The non-uniform shrinking prescribes a non-Euclidean metric on a disc, and thus a non-zero Gaussian curvature. To minimize their elastic energy the free sheets form three-dimensional structures that approximate the imposed metric. We show how both large scale buckling and wrinkling-type structures can be generated, depending on the nature of possible embeddings of the imposed metric in Euclidean space.

Keywords: Buckling; Thin plates; Elasticity; Metric; Gaussian curvature

1. Introduction

A large variety of elaborate 3D structures appear in nature as a result of the growth of seemingly unconstrained slender sheets. Examples are leaves, flowers and marine invertebrates. Can such structures result from lateral tissue growth, or should their growth be asymmetric and three dimensional? In this work we study how non-uniform lateral growth/shrinking of elastic sheets leads to the formation of non-trivial 3D configurations.

Equilibrium configurations of thin elastic sheets have been studied extensively. In most cases the study was focused on confinements of existing sheets. Such systems present different types of solutions, such as buckling [1], crumpling [2–4], blistering and wrinkling [5,6], depending on the details of the system. Recent observations showed [7–10] that multi-scale wavy structure can appear even on sheets that are *free* of any external constraint. The wavy edges of torn plastic sheets were found to form cascades of similar buckles over many length scales. The observed fractal structures corresponding to the minimum of the elastic energy of plastic sheets whose margins were stretched by the irreversible plastic deformations that accompanied the tearing showed a strong resemblance to naturally formed thin sheets such as a beet leaf [7]. Could the highly complicated forms of natural thin sheets be produced by a simple mechanism reminiscent of the featureless plastic deformation of a plastic bag?

Thin sheets are elastic bodies for which one dimension, the thickness t, is much smaller than the other lateral dimensions L. In this work we consider thin plates—thin sheets that are homogeneous through their thickness and, unlike shells, have zero spontaneous curvature. There is a 2D approximation for the elastic energy of a deformed plate—the Föppl–Von Kármán (FVK) energy functional [11]. In this approximation, though the plate is a 3D object, its energy is expressed in terms of geometrical properties of a 2D surface—the mid-surface of the plate. The energy is a sum of two terms, resulting from two types of deformations; in-plane stretching, for which all surfaces composing the plate are deformed in the same manner, and pure bending for which the mid-surface is not stretched/compressed but the surfaces above and below it are. Intrinsically, the mid-surface is characterized by its 2D metric tensor, g (see [12] for basic definitions), which is invariant under pure bending. Its *shape* is characterized by the shape operator (see [14], p. 196), whose eigenvalues are the principal curvatures, k_1 and k_2. Gauss's "Theorema Egregium" shows that the determinant of the shape operator, $k_1 k_2 \equiv K$, the Gaussian curvature, is completely defined by the metric tensor.

* Corresponding author. Tel.: +972 2 6586104; fax: +972 2 6584437.
E-mail address: erans@vms.huji.ac.il (E. Sharon).

0167-2789/$ - see front matter
doi:10.1016/j.physd.2007.04.024

Employing linear elasticity, the bending energy density of a plate is cubic in the thickness and quadratic in the principal curvatures. The stretching energy density is linear in the thickness and quadratic in the in-plane strain, which is half the difference between the metric tensors of a reference, stress-free, and current configurations (see [15], p. 1). One immediate conclusion is that for very thin plates ($t \ll L$), bending will be energetically favorable over stretching. Thus equilibrium configurations of thin sheets involve only small in-plane strains [16].

In this work we study the equilibrium configurations of growing/shrinking plates. Growing elastic bodies usually contain internal stresses [13]. Thus, when trying to express the energy of growing sheets we face the problem of defining a stress-free configuration, with respect to which strains are measured. To overcome this difficulty, we use the 2D approximation formalism and recall that our sheets are plates; thus their bending is measured with respect to a plane: The sheets are free of bending energy only in planar configurations and configurations that are symmetric with respect to a plane will have the same bending energy. To evaluate the stretching energy we recall that it results solely from in-plane strain. We, thus, do not need a (stress-free) *reference configuration*, but only a *reference metric*, with respect to which we measure the in-plane strain. We use the term "target metric", g_{tar} (see [10]), to describe a 2D metric tensor which is prescribed by the local growth. A sheet adopting a configuration satisfying g_{tar} will be completely free of in-plane strain.

We are interested in cases where local growth leads to the formation of 3D configurations. Gauss's "Theorema Egregium" provides a link between metrical properties of a surface and 3D configurations in space. It states that the local metric tensor completely determines the local Gaussian curvature on a surface. Thus, if g_{tar} is non-Euclidean, it determines non-zero "target Gaussian curvature", K_{tar}. In this case, all configurations satisfying g_{tar} cannot be flat and the two terms in the energy functional "aim" at two different types of configurations: The bending term favors completely flat configurations, while the stretching term favors 3D configurations with the metric g_{tar}. The selected configuration is set by the competition between the two. As explained before, for thin enough sheets, we expect the equilibrium configurations to be "very close" to embeddings of g_{tar}.

To conclude the introduction, the shaping scenario that we study goes as follows: Take a sheet and make it grow, swell, or shrink laterally, but non-uniformly. This process prescribes a non-Euclidean g_{tar} on the sheet, which corresponds to a non-zero target Gaussian curvature, $K_{\text{tar}} \neq 0$. To minimize its elastic energy, the sheet finds a configuration – an embedding of some metric g – that is close to g_{tar}, and thus not flat. However, buckling of plates costs bending energy that increases with curvature. The actual stable configurations are, thus, set by the competition between stretching and bending.

2. Experimental system

We have built an experimental system that allows us to use and study the mechanism discussed above. We use N-isopropylacrylamide (NIPA) gel to construct sheets with inducible non-Euclidean metrics. The gel is made by mixing NIPA monomers with bisacrylamide (BIS) (5–10% of NIPA) cross-linker in water. The addition of 1% ammonium persulfate (APS) and 0.25% tetramethyl ethylene diamine (TEMED) initiates polymerization of a cross-linked elastic hydrogel. This gel undergoes a sharp volume reduction transition at $T_c = 33\,^{\circ}\text{C}$ [17], above which its equilibrium volume decreases considerably. We measured the shrinking ratios of homogeneous gel discs of different NIPA concentration. These measurements show a strong dependence on monomer concentration: Dilute gels shrink a lot, while concentrated gels undergo a moderate volume reduction (Fig. 1). The concentration of cross-linker (within the relevant range of parameters) hardly affects the gels' shrinking ratio.

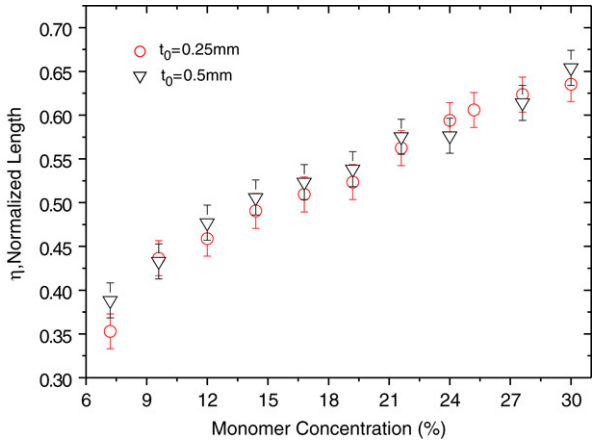

Fig. 1. The shrinking of a NIPA gel sheet as a function of its monomer concentration. The normalized length was obtained by dividing the diameter of a warm gel disc by its original diameter. Shrinking was obtained by immersing the discs into a water bath and increasing the temperature up to 45 °C over ten hours. t_0 is the thickness of the cold sheet.

We cast radial discs by injecting the NIPA solution into the gap between two flat glass plates through a center hole in one of them (a Hele–Shaw cell; Fig. 2). To impose non-Euclidean target metrics, we change the NIPA concentration during the injection. Polymerization takes place within a minute and the gradients in concentration are "frozen" within the gel. the result is a disc with internal *lateral* gradients in NIPA concentration. Monotonic gradients are generated with a passive gradient maker, while programmable actuated valves are used to inject solutions with more complicated radial gradients in monomer concentration (Fig. 2).

3. Results

The generated plates are flat below T_c, but are "programmed" to shrink with ratios $\eta(r)$ at each radius r on the disc, once the temperature is increased above T_c. This differential shrinking sets new equilibrium distances between points on the surface—it determines a new target metric, g_{tar}, on the sheet. To see the connection between the shrinking profile $\eta(r)$ and g_{tar} we consider a closed circle of radius r, on the cold disc. Following the shrinking with ratio $\eta(r)$, both perimeter and radius of the circle are modified. The perimeter that was $2\pi r$ is

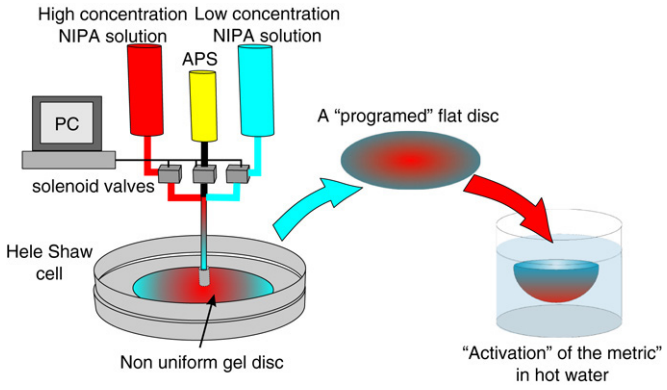

Fig. 2. Schematic of the formation of sheets with inducible non-Euclidean target metric. High and low NIPA concentration solutions are injected into a Hele–Shaw cell through programmable valves. Polymerization leads to the generation of a flat disc, having internal radial gradients in monomer concentration. Once immersed in warm water of temperature $T > T_c = 33\,^{\circ}\mathrm{C}$, it shrinks differentially, adopting a new, non-Euclidean target metric. As a result it forms a three-dimensional structure. The illustration shows a surface of positive Gaussian curvature, generated by increasing monomer concentration during the injection.

now $2\pi r\eta$. The radius is $\rho(r) = \int_0^r \eta(r')\mathrm{d}r'$. Thus, the perimeter of a circle of radius ρ on the shrunk disc is now $f(\rho)2\pi\rho$, where $f(\rho)$ is determined by $\eta(\rho)$ and its integral, and thus by the monomer concentration profile. Using a polar coordinate system, (ρ, θ), the linear element determined by g_{tar} is $\mathrm{d}l^2 = \mathrm{d}\rho^2 + \rho^2 f(\rho)^2 \mathrm{d}\theta^2$, and the prescribed (by Gauss's theorem) target Gaussian curvature reads

$$K_{\mathrm{tar}}(\rho) = -\frac{(\rho f(\rho))_{\rho\rho}}{\rho f(\rho)}. \tag{1}$$

The monomer concentration profile, which determines $\eta(\rho)$, allows us to set $(\rho f(\rho))_{\rho\rho}$ and to prescribe a target Gaussian curvature: For $(\rho f(\rho))_{\rho\rho} \neq 0$ we have $K_{\mathrm{tar}} \neq 0$. In this case, any embedding of g_{tar} cannot be flat. Indeed, sheets with increasing/decreasing monomer concentration profiles (Fig. 3) that define Gaussian curvatures, ranging from negative to positive, attain configurations that correspond to the prescribed metrics (insets in Fig. 3). The discs of $K_{\mathrm{tar}} > 0$ are buckled into dome-like shapes, while the discs of $K_{\mathrm{tar}} < 0$ are shaped into wavy structures, reminiscent of the wavy edges of torn plastic sheets. In both cases, the larger the gradients in NIPA concentration, the more curved the surfaces are.

Next we perform a quantitative comparison between the metric of the curved discs and their target metric. The topography of the discs $z(x, y)$ is measured using an optical profilometer (Conoscan 3000; inset of Fig. 4) with a resolution of 25 μm in the lateral, x and y, directions and 5 μm in the vertical, z, direction. In order to identify points of a given distance ρ from the center, we re-parameterize the surface onto a semi-geodesic coordinate system $z(\rho, \theta)$. First we plot radial geodesics (the equivalent of radial lines on a curved surface) at azimuthal angles θ, by solving the geodesic equation (see [12]) from a central circle. The points at distance ρ on these geodesics form a circle of radius ρ on the surface (in general, these are not circles in the x, y plane). Measurements of the perimeters of circles of radius ρ on the surface are

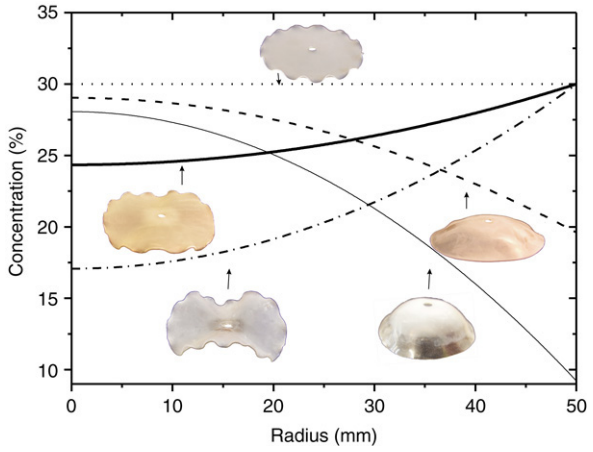

Fig. 3. The control over the discs' curvature. The NIPA concentration as a function of radius on the cold discs (all discs are of initial thickness $t_0 = 0.5$ mm). Discs with NIPA concentration that increases with radius (dot–dashed, bold line) result in the prescription of $K_{\mathrm{tar}} < 0$ and the formation of wavy configurations (left insets). A flat concentration profile (dotted) results in $K_{\mathrm{tar}} = 0$, and thus a flat disc (upper inset), while a decreasing concentration profile defines $K_{\mathrm{tar}} > 0$, resulting in the formation of dome-like structures (right insets). The contact of the discs' margins with air during polymerization leads to the formation of a narrow region of $K_{\mathrm{tar}} < 0$, resulting in the formation of the observed short wavelength waviness along the margins of the disc of $K_{\mathrm{tar}} = 0$.

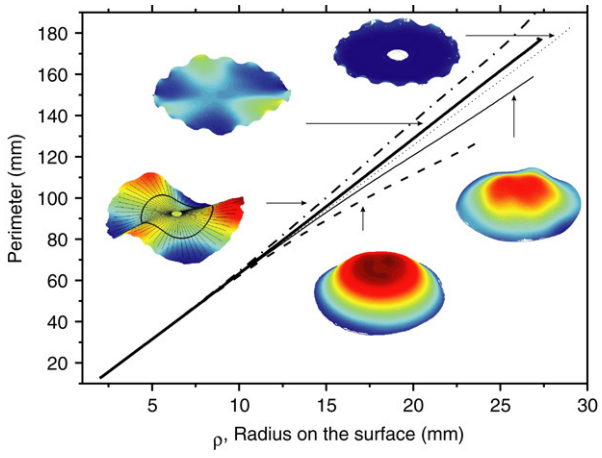

Fig. 4. The metric of the curved discs. The perimeter of a circle on the surface of a disc, as a function of its radius (both measured along the surface; lines as in Fig. 3). The surface topography measurements (insets) are "placed" on a semi-geodesic coordinate system, allowing the identification of points of a given radius ρ, as illustrated for a surface of $K_{\mathrm{tar}} < 0$ (bottom left inset; the full color range spans 14 mm). Integration of the length of such circles yields the perimeter at ρ. As expected, for the flat disc (dotted) the perimeter equals $2\pi\rho$, while for the discs of $K_{\mathrm{tar}} < 0/ > 0$ the perimeter increases faster/slower than linearly. The presented data do not include the narrow wavy strips along the discs' margins.

presented in Fig. 4. In accordance with the target metric, for discs of $K_{\mathrm{tar}} > 0$ the perimeter increases with ρ slower than linearly, while for $K_{\mathrm{tar}} < 0$ it increases faster than linearly. A quantitative comparison of the perimeter at ρ to $f(\rho)2\pi\rho$ is presented for the surfaces of smallest and largest K_{tar} (Fig. 5). In both cases, the perimeter at ρ closely follows the prescribed one, and indeed the sheets' metric (averaged over θ) is very

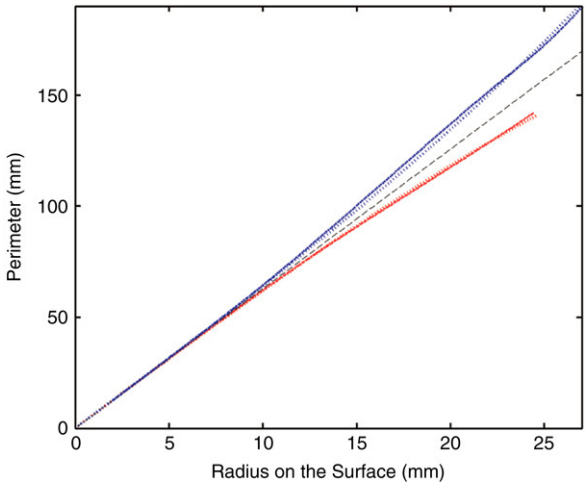

Fig. 5. A quantitative comparison between g_{tar} and the generated metric. Disc perimeter as a function of ρ (solid lines) compared to the perimeter prescribed by the input metric, g_{tar} (dashed lines). Both positive (red) and negative (blue) Gaussian curvature discs "follow", on average, their input metric. The dashed black line indicates a flat disc, for which the perimeter equals $2\pi\rho$. (For interpretation of the references to colour in this figure legend, the reader is referred to the web version of this article.)

close to its target metric. One can, thus, generate various 3D structures using systematic control over their target metrics.

Intrinsically, the discs of $K_{tar} > 0$ and $K_{tar} < 0$ are very similar, generated by just inverting the NIPA concentration profiles (Fig. 3). Their shapes, on the other hand, are qualitatively different. The sheets of positive Gaussian curvature preserve the axial symmetry of g_{tar}, as they are shaped into surfaces of revolution. In contrast, the discs of $K_{tar} < 0$ break this symmetry, selecting wavy configurations. One would wonder what the origin of this difference is. Why would a free sheet with radially symmetric target metric select a wavy equilibrium configuration that breaks this symmetry? We suggest that the difference results from the limitations on possible embeddings of the given target metrics in Euclidean space. Radially symmetric embeddings of discs with $K > 0$ exist and the sheets use them as a base for energy minimizers. However, embedding a disc with radially symmetric hyperbolic metric (having $K_{tar} < 0$) in Euclidean space is non-trivial. To our knowledge such embeddings should involve small scale structure, which is associated with large bending energy. The larger the sheet is, the smaller this scale should be [18,19]. This prevents the sheets from settling "close to" an embedding of g_{tar}. Instead, they select a wrinkling-type behavior to minimize their energy. This behavior is reminiscent of wrinkling in constrained systems [6,20,21]. There, boundary conditions exclude the existence of any low bending stretch-free configuration, and small scale, or multi-scale wrinkling is the way to minimize energy. Apparently, once considering certain non-Euclidean metrics, these conditions can be met even with unconstrained sheets.

In summary, we have constructed elastic sheets with non-Euclidean target metrics, g_{tar}. To minimize their elastic energy these free sheets spontaneously form non-trivial 3D structures. We have shown the qualitative and quantitative control over sheets' configurations, by adjustments of g_{tar}. The sheets with $K_{tar} > 0$ buckle into large scale symmetric configurations, while sheets with $K_{tar} < 0$ select wavy configurations. We suggest that these different deformation modes are selected based on limitations on possible embeddings of the imposed metrics in Euclidean space. The shaping principle, presented here, might play a role during developmental processes in naturally growing sheets. In such systems, the local nature of the growth might lead to the formation of non-Euclidean metrics. In this case the sheets can take elaborate global configurations, having non-uniform in-plane strain distribution. In our experimental system, g_{tar} can be turned "on" and "off" by environmental conditions. This characteristic, which has an applicative potential, can be implemented with other artificial materials that undergo large volume reduction. Materials that respond to light [22], pH [23], glucose level [24] and other chemical signals [17] were developed and are good candidates for implementation of the principle we presented. Further study of the principles of shaping by metric prescription can extend the types and variety of structures that can be formed using thin sheets, as well as improving our understanding of developmental processes.

Acknowledgments

This research was supported by GIF, BSF and the EEC MechPlant NEST.

References

[1] B. Roman, A. Pochau, Euro. Phys. Lett. 46 (1999) 602.
[2] E.A. Lobkovsky, A.T. Witten, Phys. Rev. E 55 (1997) 1577.
[3] K. Matan, R. Williams, T. Witten, S. Nagel, Phys. Rev. Lett. 88 (2002) 076101.
[4] Y. Pomeau, Phil. Mag. B 78 (1998) 235.
[5] M. Ortiz, G. Gioia, J. Mech. Phys. Solids 42 (1994) 531.
[6] E. Cerda, L. Mahadevan, Phys. Rev. Lett. 90 (2003) 074302.
[7] E. Sharon, B. Roman, M. Marder, H. Swinney, Nature 419 (2002) 579.
[8] M. Marder, E. Sharon, B. Roman, S. Smith, Euro. Phys. Lett. 62 (2003) 498.
[9] B. Audoly, A. Boudaoud, Phys. Rev. Lett. 91 (2003) 086105.
[10] M. Marder, N. Papanicolaou, J. Stat. Phys. (2005).
[11] A. Föppl, Vorlesungen ü. technische Mechanik, 5th ed., Leipzig, 1907.
[12] A.V. Pogorelov, Differential Geometry, P. Noordhoff N. V., Groningen, The Netherlands, 1956.
[13] A. Goriely, M. Ben Amar, Phys. Rev. Lett 94 (2005) 198103.
[14] B. O'Neill, Elementary Differential Geometry, Academic Press, New York, 1966.
[15] L.D. Landau, E.M. Lifshitz, Theory of Elasticity, Pergamon Press, Oxford, New York, 1970.
[16] A. Pogorelov, Bending of Surfaces and Stability of Shells, American Mathematical Society, Providence, 1988.
[17] T. Tanaka, Phys. Rev. Lett. 40 (1978) 820.
[18] G.E. Poznyak, V.E. Shikin, Amer. Math. Soc. Transl. 176 (1996) 151.
[19] R.E. Rozendorn, Encyclopaedia of Mathematical Sciences—Geometry III, vol. 48, 1992, p. 89.
[20] K. Efimenko, M. Rackaitis, E. Manias, A. Vaziri, L. Mahadevan, J. Genzer, Nat. Mater. 4 (2005) 293.
[21] N. Bowden, S. Brittain, A. Evans, W.J. Hutchinson, M.G. Whitesides, Nature 393 (1998) 146.
[22] A. Lendlein, H. Jiang, O. Junger, R. Langer, Nature 434 (2005) 879.
[23] O. Philippova, D. Hourdet, R. Audebert, A. Khokhlov, Macromolecules 30 (1997) 8278.
[24] K. Kataoka, H. Miyazaki, M. Bunya, T. Okano, Y. Sakurai, J. Am. Chem. Soc. 120 (1998) 12694.